bioRxiv preprint doi: https://doi.org/10.1101/736330; this version posted March 13, 2020. The copyright holder for this preprint (which was not certified by peer review) is the author/funder. All rights reserved. No reuse allowed without permission.

# MicroRNA profiles in calcified and healthy aorta: therapeutic impact of miR-145 and miR-378

**Running title:** *miRNA replacement in aortic calcification*

Ying Tang[1, †], Tapan A. Shah[1, †, ‡], Edward J. Yurkow[2], and Melissa B. Rogers[1, ‡]

[1]Rutgers - New Jersey Medical School, Microbiology, Biochemistry, & Molecular Genetics, Newark, NJ

[2]Rutgers University Molecular Imaging Center (RUMIC), Rutgers University, Piscataway, NJ

[†]Co-first authors

[‡]Present Address: Advanced Cell Diagnostics, 7707 Gateway Blvd #200, Newark, CA 94560

[§]To whom should correspondence and reprint request be addressed to: Melissa B. Rogers, Ph.D., Microbiology, Biochemistry & Molecular Genetics, Rutgers - NJ Medical School (NJMS), Center for Cell Signaling, Room F1216, 205 South Orange Ave., Newark, NJ 07103. Email: rogersmb@njms.rutgers.edu, telephone: 973 972 2984

**Acknowledgements:** We warmly thank Youhua Zhu for her diligent technical assistance, Dr. Diane Garsetti and Yue Wang for critically reading the manuscript, and Lindsey Hernandez for bioinformatics assistance. We appreciate the technical assistance provided by the NJMS Genomics Center.

Funding was provided by grants from the National Heart, Lung, and Blood Institute (R01HL114751) and National Institutes of Aging (R56AG050762) and from the NJMS Research Core Facilities Matching Funds Small Grants Program to MBR and an American Heart Association fellowship (20POST35210235) to YT.

**Conflict of Interest statement:** The authors declare that they have no conflicts of interest with the contents of this article.

bioRxiv preprint doi: https://doi.org/10.1101/736330; this version posted March 13, 2020. The copyright holder for this preprint (which was not certified by peer review) is the author/funder. All rights reserved. No reuse allowed without permission.



## Abstract

Our goal was to elucidate microRNAs (miRNAs) that may repress the excess bone morphogenetic protein (BMP) signaling observed during pathological calcification in the *Klotho* mouse model of kidney disease. We hypothesized that restoring healthy levels of miRNAs that post-transcriptionally repress osteogenic calcific factors may decrease aortic calcification. Our relative abundance profiles of miRNAs in healthy aorta differ greatly from those in calcified mouse aorta. Unbiased analyses of KEGG and GO term associated genes suggest that these miRNAs regulate proteins involved in many essential processes, including osteogenesis. Two differentially regulated miRNAs, miR-145 and miR-378, were selected based on three criteria: reduced levels in calcified aorta, the ability to target more than one protein in the BMP signaling pathway, and conservation of targeted sequences between humans and mice. Forced expression using a lentiviral vector demonstrated that restoring normal levels repressed the synthesis of BMP2 and other pro-osteogenic proteins and inhibited pathological aortic calcification in mice with renal insufficiency. This study identified miRNAs that may impact BMP signaling in both sexes and demonstrated the efficacy of selected miRNAs in reducing aortic calcification *in vivo*. Calcification of the aorta and the aortic valve resulting from abnormal osteogenesis is common in those with kidney disease, diabetes, and high cholesterol. Such vascular osteogenesis is a clinically significant feature. The calcification modulating miRNAs described here are candidates for biomarkers and “miRNA replacement therapies” in the context of chronic kidney disease and other pro-calcific conditions.

**Keywords:** bone morphogenetic proteins, gene regulation, signal transduction, cardiovascular system, vascular calcification, renal insufficiency, microRNA

bioRxiv preprint doi: https://doi.org/10.1101/736330; this version posted March 13, 2020. The copyright holder for this preprint (which was not certified by peer review) is the author/funder. All rights reserved. No reuse allowed without permission.



## Introduction

The American Heart Association projects that 45% of Americans will have some form of heart and/or vascular disease by 2035 (Benjamin *et al.*, 2019). Calcification of blood vessels reduces their diameter and plasticity and ultimately promotes ischemic events (Karwowski *et al.*, 2012). Risk factors that promote both vascular and valvular calcification include aging, renal failure, and male sex; as well as hypercholesterolemia, smoking, and diabetes (Towler, 2017; Yutzey *et al.*, 2014). An aging population and the epidemic of obesity ensure that cardiovascular disorders will be a major public health threat for decades to come. Understanding the signaling processes that regulate the behavior of vascular cells will reveal novel approaches to preventing and treating these devastating pathologies. Here we focused on identifying microRNAs (miRNAs) that regulate pathological cardiovascular calcification.

The BMP signaling pathway is essential for osteogenesis and vascular calcification (Bostrom *et al.*, 2011; Garcia de Vinuesa *et al.*, 2016; Towler, 2017). BMP ligands bind BMP receptors (BMPR), which phosphorylate and activate SMAD signaling. SMAD signaling increases transcription of *Runx2* and *Msx2*, leading to increased osteogenic differentiation (Garcia de Vinuesa *et al.*, 2016; Leopold, 2012; Towler, 2017). Abnormally elevated levels of the pro-osteogenic bone morphogenetic protein 2 (BMP2) and increased BMP signaling are implicated in all forms of pathological cardiovascular calcification. For example, BMP2 is synthesized in human atherosclerotic plaques (Bostrom *et al.*, 1993) and calcified stenotic valves (Nagy *et al.*, 2013). Moreover, BMP2 can induce master osteogenic factors such as RUNX2 in human aortic valve interstitial cells (X. Yang *et al.*, 2009) and MSX2 in aortic smooth muscle cells (Cheng *et al.*, 2003), induce calcification *in vitro* (Nigam & Srivastava, 2009; Osman *et al.*, 2006; Wirrig *et al.*, 2011; X. Yang *et al.*, 2009; Z. Yu *et al.*, 2011), and cause ossification within adult diseased valves (Miller *et al.*, 2010; Mohler *et al.*, 2001; Wirrig *et al.*, 2011) and atherosclerotic plaques (Bostrom *et al.*, 1993). Forced synthesis of BMP2 in vascular smooth muscle cells accelerated atherosclerotic calcification in *ApoE* null mice fed a high cholesterol diet (Nakagawa *et al.*, 2010). Genetic deficiency and pharmacological inactivation of BMP signaling reduced calcification not only in cultured cells (Balachandran *et al.*, 2010; Gomez-Stallons *et al.*, 2016; Wirrig *et al.*, 2011) but also in *Ldlr* null mice fed a high-fat diet (Derwall *et al.*, 2012), *Mgp* null mice (Malhotra *et al.*, 2015) and *Klotho* mutant mice with renal failure (Gomez-Stallons *et al.*, 2016).

Given the importance of BMP signaling in cardiovascular calcification, identifying post-transcriptional regulators of BMP signaling may provide new insights and targets for the treatment of cardiovascular disease. To increase potential clinical translatability, we also considered evolutionary conservation. The 3'-untranslated region (3'-UTR) of messenger RNAs (mRNAs) binds regulatory proteins and miRNAs that influence polyadenylation, translation efficiency, and stability of mRNAs (Corbett, 2018). All BMP ligands may be post-transcriptionally regulated. However, the extreme evolutionary conservation of the *Bmp2* 3'-UTR relative to other BMP ligand 3'-UTRs supports a potentially greater role for post-transcriptional mechanisms that are conserved between mouse and man (Fotinos *et al.*, 2016; Rogers *et al.*, 2015; Shah *et al.*, 2017). MicroRNAs are crucial regulators in cardiovascular pathologies (Johnson, 2019). The goal of this study was to compare the profiles of miRNAs that modulate the

bioRxiv preprint doi: https://doi.org/10.1101/736330; this version posted March 13, 2020. The copyright holder for this preprint (which was not certified by peer review) is the author/funder. All rights reserved. No reuse allowed without permission.



synthesis of BMP2 and downstream BMP signaling proteins in the aorta of healthy mice relative to mice with pathologically calcified aorta. Our mouse model is a *Klotho* hypomorph that causes dysregulated mineral metabolism (Kuro-o *et al.*, 1997).

The phenotype of mice homozygous for *Klotho* mutations includes a short lifespan, atherosclerosis, ectopic calcification, and renal disease. The KLOTHO protein, along with 1,25$(OH)_2$ vitamin D3 and FGF23, tightly regulates phosphate homeostasis (Hu *et al.*, 2011; Yamada & Giachelli, 2017). Deficiency of KLOTHO leads to renal disease and subsequent hyperphosphatemia and ectopic calcification of soft tissues such as aorta, aortic valves and kidneys (Gomez-Stallons *et al.*, 2016; Yamada & Giachelli, 2017). Restoration of normal KLOTHO levels ameliorates calcification (Hu *et al.*, 2011). The dramatic calcification of the aorta and other tissues in *Klotho* mutant mice within 6-7 weeks of birth make them experimentally attractive for studying gene regulation and signaling changes during pathological calcification. Understanding the mechanism of aortic calcification in the context of kidney failure is important because 17% of the population over the age of 30 may suffer from this major cardiovascular disease risk factor by 2030 (Benjamin *et al.*, 2019).

Our objective was to elucidate a comprehensive profile of miRNAs whose abundance is altered in the calcified aorta of *Klotho* homozygous mutant mice with renal disease. Our miRNA profiles from both male and female healthy and diseased mice reflect the extensive changes that occur during vascular disease. Here we discuss the subset of differentially regulated miRNAs that may impact the pathological osteogenesis that contributes to vascular calcification. We also demonstrate that selected miRNAs can modulate the BMP2 ligand and proteins involved in BMP signaling and calcification *in vivo*. Finally, we provide proof-of-principle evidence that increasing the abundance of miRNAs that inhibit BMP signaling can ameliorate aortic calcification. This study begins to fill a key gap in our understanding of post-transcriptional processes that control BMP signaling and calcification in vascular tissues and provides experimental support for miRNA replacement therapies in cardiovascular disease.

## Experimental procedures

### *Tissue collection*

Mice bearing the *Klotho* mutation were a gracious gift from Dr. Makoto Kuro-o (Jichi Medical University) by way of Dr. Sylvia Christakos (Rutgers New Jersey Medical School). The mice were a mixture of strains FVB, C57Bl/6J, and C3H/J. Because homozygous *Klotho* null mice are infertile, mice were maintained by heterozygous-by-heterozygous mating. 25% of each litter was homozygous and exhibited the full *Klotho* phenotype, including ectopic soft tissue calcification. 50% were heterozygous and 25% were wild type. No statistically significant differences in any parameter were observed between mice bearing the heterozygous and wild type *Klotho* genotypes (Table S1). Assessed parameters included body and organ weights, gene expression, and calcium levels. Because our analyses were consistent with published data indicating that the *Klotho* mutation is fully recessive, heterozygous and wild type samples were presented together as “healthy control” samples.

bioRxiv preprint doi: https://doi.org/10.1101/736330; this version posted March 13, 2020. The copyright holder for this preprint (which was not certified by peer review) is the author/funder. All rights reserved. No reuse allowed without permission.



All animal procedures were in accordance with the guidelines for Care and Use of Experimental Animals and approved by the NJ Medical School Institutional Animal Care and Use Committee (IACUC protocol #PROTO999900898). Control and *Klotho* homozygote mice were fed regular chow and euthanized at 50 $\pm$ 1 days of age. After weaning, *Klotho* homozygotes received softened chow on the floor of the cage. On the day of necropsy, mice were killed with an inhalation overdose of isoflurane. Immediately thereafter, the heart was perfused *via* the left ventricle with phosphate buffered saline (PBS, pH 7.3), to remove excess blood. The aorta including the ascending aorta, arch and descending thoracic aorta was removed. After cutting at the surface of the heart, the aorta was rinsed in PBS, blot dried and weighed. The aorta was snap-frozen in liquid nitrogen and stored at -80°C. Frozen tissues were ground in liquid nitrogen using a mortar and pestle. To facilitate handling small tissues such as the diseased aortas from *Klotho* homozygotes, acid-washed glass beads (Millipore-SIGMA, St. Louis, MO, # G1277) were added during the grinding. Glass beads did not affect the biochemical assays (Fig. S1A, B).

### *Western Blots*

Frozen ground tissue was solubilized in RIPA buffer, sonicated, and subjected to western blot analyses as described in Shah *et al.* (Shah *et al.*, 2017). BMP signaling was measured using a monoclonal phospho-SMAD 1/5/9(8) antibody (Cell Signaling Technology, Danvers, MA, #13820) at a dilution of 1:1000. The pSMAD antibody was authenticated as described in Fig. S1C and D. Polyclonal total SMAD 1/5/9(8) (Santa Cruz Biotechnology, Inc., Santa Cruz, CA, #sc-6031-R) and a polyclonal actin antibody (Santa Cruz Biotechnology, Inc., Santa Cruz, CA, #sc-1615-R) were subsequently used at a dilution of 1:1000. In all cases, the secondary antibody was Goat Anti-Rabbit HRP (Abcam, Cambridge, MA, # ab97080) at a dilution of 1: 20,000. Antibody-bound proteins were detected using SuperSignal™ West Femto Maximum Sensitivity Substrate (ThermoFisher Scientific, Waltham, MA, # 34096) and imaged using a FluoroChem M (Protein Simple, San Jose, California).

### *Calcium assays*

Ground tissue was solubilized and lysed by sonication on ice in PBS, pH 7.3 containing 0.16 mg/mL heparin. The Cayman Chemical Calcium Assay kit was used to measure calcium levels (Ann-Arbor, MI, #701220). Calcium levels were normalized to protein levels measured using the Bradford assay (Bio-Rad Laboratories, Hercules, CA, # 5000006).

### *Spatial mapping of calcified structures*

The patterns of mineralization in *Klotho* heterozygote *vs. Klotho* mutant mice were determined using microcomputerized tomography (microCT) at the Rutgers Molecular Imaging Center (http://imaging.rutgers.edu/). Mice were scanned using the Albira® PET/CT (Carestream, Rochester, NY) at standard voltage and current settings (45kV and 400μA) with a minimal voxel size of <35 μm. Voxel intensities in the reconstructed images were evaluated and segmented with VivoQuant image analysis software (version 1.23, inviCRO LLC, Boston).

### *MicroRNA microarray and data analysis*

bioRxiv preprint doi: https://doi.org/10.1101/736330; this version posted March 13, 2020. The copyright holder for this preprint (which was not certified by peer review) is the author/funder. All rights reserved. No reuse allowed without permission.



Aortic samples were obtained from both male and female control and *Klotho* mutant mice at 7 to 8 weeks of age (Table 1). RNA was extracted using the miRNeasy Mini Kit (Qiagen Inc., Germantown, MD, # 217004). The RNA quality was checked using a Bioanalyzer (Agilent Technologies, Santa Clara, CA).

MicroRNA expression in the aorta was assessed with the Applied Biosystems™ GeneChip™ miRNA 4.0 Array (ThermoFisher Scientific, Waltham, MA, #902412) in the Rutgers NJMS Genomics Center. The GeneChip™ miRNA 4.0 Array contained the miRNAs and pre-miRNAs (precursors to the miRNAs) listed in the Sanger miRBase v20. The miRNA arrays were processed following the manufacturer's instructions. Briefly, using the Applied Biosystems™ FlashTag™ Biotin HSR RNA Labeling Kit (ThermoFisher Scientific, Waltham, MA, the # 902446), 400 ng of total RNA was labeled with biotin and hybridized to the miRNA 4.0 Array (ThermoFisher Scientific, Waltham, MA, #902412) for 18 hours at 48°C using an Affymetrix® 450 Hybridization Oven (Affymetrix, Santa Clara, CA). After washing and staining on an Affymetrix® 450 Fluidics Station (Affymetrix, Santa Clara, CA), using the Applied Biosystems™ GeneChip™ Hybridization, Wash, and Stain Kit (ThermoFisher Scientific, Waltham, MA, #900720), the arrays were scanned using the Affymetrix® Scanner 3000 7G (Affymetrix, Santa Clara, CA). CEL files were generated using the Affymetrix data extraction protocol in the Affymetrix GeneChip® Command Console® Software (Affymetrix, Santa Clara, CA, USA). The resulting CEL files (GSE135759) were analyzed using the Transcriptome Analysis Console 4.0 (TAC, ThermoFisher Scientific, Waltham, MA ), including the Robust-Multi-array Average algorithm to correct for microarray background and to normalize miRNA expression profiles on a log scale. TAC's ANOVA analysis identified the miRNAs whose abundance differed significantly between control and *Klotho* homozygous mutant mice. Minimal significance was defined as a *p* value of 0.05.

### *Bioinformatic analyses*

MicroRNAs that significantly down-regulated in both sexes of *Klotho* homozygous mice compared to control were further used to perform target prediction (see microarray data analysis). Predicted target profiles were obtained from the DNA Intelligent Analysis (DIANA)-micro T-CDS (v. 5.0) which permits the entry of multiple miRNAs simultaneously (http://www.microrna.gr/webServer) (Paraskevopoulou *et al.*, 2013). The micro T-CDS threshold score for predicted targets was set at 0.6. Scores ranged from 0 to 1, with a higher score indicating an increased probability of a true microRNA target. To classify and visualize the biological processes affected by the target genes predicted by DIANA, Gene Ontology (GO) and KEGG (Kyoto Encyclopedia of Genes and Genomes) were utilized with the R package, clusterProfiler (http://bioconductor.org/packages/release/bioc/html/clusterProfiler.html) (G. Yu *et al.*, 2012). Minimal significance was defined as a *p* value of 0.05. Alignments between selected miRNAs and mouse genes were predicted by MiRanda (Betel *et al.*, 2008) and TargetScan 7.2 (http://www.targetscan.org/mmu_72/ (Agarwal *et al.*, 2015)).

### *Real-Time Reverse Transcription PCR for detection of microRNA-145 and microRNA-378a and target gene expression*

bioRxiv preprint doi: https://doi.org/10.1101/736330; this version posted March 13, 2020. The copyright holder for this preprint (which was not certified by peer review) is the author/funder. All rights reserved. No reuse allowed without permission.



MicroRNA cDNA was synthesized using the miScript PCR Kit (Qiagen Inc., Germantown, MD, # 218073). The miScript PCR kit utilized a universal oligo-dT primer tag to convert all RNA species (total RNA and miRNA) into cDNA. A universal reverse primer supplied with the miScript PCR kit was used to amplify cDNA from each miRNA. The miRNA forward primers were designed based on miRNA sequences in miRBase 22 (http://www.mirbase.org/). GCG or CGC was added to the 5' end of the primers when the GC % was low. NCBI nucleotide blast was used to confirm the absence of non-specific binding sites for the forward primers. Messenger RNA (mRNA) cDNA was synthesized using the QuantiTect® Reverse Transcription kit (Qiagen Inc., Germantown, MD, # 205313). Intron-spanning primers for mRNA were used to eliminate amplicons generated from any contaminating genomic DNA. Primer sequences are shown in Table 2.

Quantitative PCR was performed on a CFX96 Touch™ Real-Time PCR Detection System (Bio-Rad Laboratories, Hercules, CA, #1855196) using the QuantiTect® SYBR® Green PCR kit (Qiagen Inc., Germantown, MD, #204145) under the following conditions: 15 min at 95°C, 39 cycles of 15 seconds at 94°C, 30 seconds at 55°C and 30 seconds 70°C. MicroRNA abundance was normalized to U6 and mRNA expression was normalized to actin. The human U6 primer used in this experiment was included in the miScript Primer assay kit (Qiagen Inc., Germantown, MD, #218300).

### *Lentiviral microRNA-145 and microRNA-378a transduction*

A lentivirus vector expressing mir-145 or mir-378a under the control of the vascular smooth muscle cell (VSMC)-specific mSm22a promoter was purchased from Biosettia (Biosettia Inc, San Diego, CA). The negative control was the empty virus vector. Newly weaned *Klotho* mutant homozygotes were injected with empty lentivirus or lentivirus bearing mir-145 or mir-378a *via* their tail veins on 5 alternate days. The total lentivirus achieved in each mouse at the end of the treatment window was $4\times10^5$ pfu/g body weight. The mir-145 lentivirus generates two mature miRNAs: miR-145a-5p and miR-145a-3p. The mir-378a lentivirus generates two mature miRNAs: miR-378a-5p and miR-378a-3p.

### *Statistical Analysis*

Data are presented as mean ± Standard Error Measurement (SEM) or Standard Deviation (SD) as indicated and analyzed with GraphPad (version 7; GraphPad Software Inc, La Jolla, CA). Statistical significance was assessed with either the Student's two-tailed t-test or one-way ANOVA. Differences were considered significant if $p<0.05$.

## Results

### *BMP signaling and calcification is elevated in aorta from Klotho homozygous mutant mice*

BMP signaling is required for valve calcification in *Klotho* null mice (Gomez-Stallons *et al.*, 2016). We assessed BMP signaling in the calcified aorta of mice homozygous for the original hypomorphic *Klotho* allele (Kuro-o *et al.*, 1997). BMP signaling and calcium levels in aorta from control mice that were either wild type ($Kl^{+/+}$) or heterozygous ($Kl^{kl/+}$)

bioRxiv preprint doi: https://doi.org/10.1101/736330; this version posted March 13, 2020. The copyright holder for this preprint (which was not certified by peer review) is the author/funder. All rights reserved. No reuse allowed without permission.



for the *Klotho* mutation were compared to the aorta from *Klotho* mutant homozygotes ($Kl^{kl/kl}$). BMP signaling, as assessed by phosphorylation of BMP-specific SMADs, was induced nearly 2-fold in aorta from male and female *Klotho* homozygous mice relative to control mice (Fig. 1A, B; $p = 0.002$). Calcium levels in the aorta from *Klotho* mutant homozygotes also were elevated by over 2-fold relative to control aorta (Fig. 1C, $p<0.0001$). PET-CT imaging revealed profound mineralization in the aortic sinus and ascending aorta of *Klotho* mutant ($Kl^{kl/kl}$) mice, but not in a control heterozygous ($Kl^{kl/+}$) littermate (Fig. 1D, E). Together, these results confirmed that homozygosity for the hypomorphic *Klotho* mutation amplifies BMP signaling and calcification in the aorta.

We then tested the hypothesis that increased abundances of aortic RNAs encoding the ligand BMP2 or the BMP signaling intermediaries SMADs 1, 5, or 9 accounted for the increased signaling in the *Klotho* homozygotes. The levels of the *Bmp2* and *Smad1* RNAs were similar to those in control mice (Fig. 2A, B). In contrast, *Smad5* and *9* RNA levels were 1.4 fold and 3.0 fold higher, respectively, in the aorta of *Klotho* homozygotes compared to control mice (Fig. 2C, D, $p < 0.05$ and $p < 0.01$). Although we have yet to rule out differential translation of the *Bmp2* and *Smad1* RNAs, we did not observe disease-associated differences in mRNA abundances. However, the increased abundance of the RNAs encoding the SMAD5 and 9 intracellular BMP signaling intermediaries indicates that increased transcription and/or stability of messages that encode BMP signaling proteins occurs in the aorta of *Klotho* mutant homozygotes.

### *MicroRNA profiles differ in the aorta from Klotho homozygous mutant mice*

BMP signaling and calcium levels are doubled in the aorta of Klotho homozygotes (Fig. 1). Alterations in miRNAs that target pro-calcific ligands such as BMP2 or signal intermediaries such as the SMADs may alter translational efficiency or destabilize mRNAs leading to changes in abundance. Consequently, we hypothesized that miRNA profiles differ in aorta from healthy control mice and *Klotho* homozygous mutant mice with renal disease. To identify miRNAs involved in aortic calcification, we profiled miRNAs in aortas from control healthy and *Klotho* mutant homozygotes. In total, 133 miRNAs were significantly increased, and 112 miRNAs were significantly decreased in *Klotho* mutant homozygous males relative to control mice ($p<0.05$, Fig. 3A, Table 3, Table S2, GSE135759). In *Klotho* mutant females, 100 miRNAs were significantly increased, and 58 miRNAs were significantly decreased ($p<0.05$, Fig. 3B, Table 3, Table S2, GSE135759). These results are consistent with a major role for miRNA-mediated post-transcriptional regulation in aortic calcification.

### *Differentially expressed miRNAs in Klotho mutant mice target osteogenic differentiation*

We hypothesized that miRNAs that are differentially expressed in the calcified aortas of *Klotho* mutant mice may affect processes related to osteogenesis. In total, the abundance of 24 miRNAs was altered significantly in both male and female *Klotho* homozygous mutant mice relative to control mice ($p<0.05$, Fig. 3C, Table 4). Of these 9 miRNAs were up-regulated and 9 miRNAs were down-regulated in both sexes of *Klotho* homozygous mice.

Curiously, the abundances of 6 miRNAs were altered by *Klotho* homozygosity but in the opposite directions in each sex: miR-7019-5p, miR-3069-3p, miR-7685-3p and miR-

bioRxiv preprint doi: https://doi.org/10.1101/736330; this version posted March 13, 2020. The copyright holder for this preprint (which was not certified by peer review) is the author/funder. All rights reserved. No reuse allowed without permission.



679-5p were up-regulated in males and down-regulated in females, whereas miR-17-5p and miR-181c-3p were down-regulated in males and up-regulated in females (Table 4). The focus of this study was to restore natural repressive mechanisms whose weakening may contribute to pathological calcification. Therefore, we focused on miRNAs whose abundance is reduced in the calcified aorta of both sexes.

We used KEGG pathways and GO molecular function terms to computationally assign the potential roles of 9 down-regulated miRNAs (Fig. 4). Similar unbiased analyses of all differentially regulated miRNAs in each sex are shown in Figures S2-5. Many key processes were enriched among the predicted target genes including signaling pathways involved in osteogenic differentiation: TGF-beta signaling (SMADs) pathways (Garcia de Vinuesa *et al.*, 2016), MAPK, PI3K-Akt (Guntur & Rosen, 2011), HIPPO, WNT/beta-catenin and the AGE-RAGE signaling pathway in diabetic complications (Kay *et al.*, 2016). A manually compiled list of BMP signaling-relevant genes predicted by TargetScan to be targeted by selected miRNAs are shown in Table S3. Together, these results suggest the disease-associated miRNA profile in *Klotho* homozygotes may influence the tendency of aortic cells to undergo osteogenic differentiation. We postulate that microRNAs that target more than one member of the BMP signaling pathway may inhibit BMP signaling by coordinately down-regulating multiple proteins and effectively restrain pathological calcification.

### *MicroRNA-145 and microRNA-378a attenuation in Klotho mutant mice*

We selected two microRNAs to test the principle that a miRNA targeting several members of the BMP signaling pathway would reduce KLOTHO deficiency-associated calcification. Two miRNAs were selected whose abundance was reduced in Klotho mutants. To increase the potential for translational studies, each was predicted to target sequences within the transcripts encoding BMP2 and SMAD proteins that are conserved between mice and humans (Table 5).

The abundance of miR-378a-5p, was sharply decreased in both male and female *Klotho* mutant mice (53% and 38% respectively, Table 4, Table S2). RT-PCR validated our microarray results and confirmed that the abundance of miR-378a-5p and -3p in *Klotho* mutant mice was half that present in healthy control aorta (Fig. 5C, D). This miRNA was predicted to target both *Bmp2* and *Smad5*. Published reporter gene studies confirmed that miR-378 directly regulates *Bmp2* (Hou *et al.*, 2012; Y. J. Yang *et al.*, 2019). The circulating level of miR-378 is reduced in the plasma of patients with coronary heart disease (Benjamin *et al.*, 2019) which is consistent with a role in cardiovascular calcification.

Our microarray measurements showed that the abundance of miR-145a-5p was reduced by 20% in male *Klotho* homozygous mutant mice as compared to healthy control mice (Table S2). RT-PCR indicated that levels of both miR-145a-5p and -3p were significantly reduced in *Klotho* mutant mice of both sexes (Fig. 5A, B). We selected this miRNA for further assessment because, miR-145a is predicted to target *Bmp2*, *Smad1*, *5* and *9* (Table 5, Table S3, (Vacante *et al.*, 2019)), was also down-regulated in *ApoE* null female mice with partial nephrectomy (Taibi *et al.*, 2014), and improves atherosclerotic symptoms in a mouse model of hyperlipidemia (Lovren *et al.*,

bioRxiv preprint doi: https://doi.org/10.1101/736330; this version posted March 13, 2020. The copyright holder for this preprint (which was not certified by peer review) is the author/funder. All rights reserved. No reuse allowed without permission.



2012). The experiments described below test the impact of restoring miR-145 abundance in an alternative setting of kidney failure with accelerated aging.

### *Forced overexpression of mir-145 and mir-378a in Klotho mutant mice*

We used a vascular smooth muscle cell (VSMC)-specific *mSm22a* promoter-driven lentivirus to increase the abundance of miR-145 and miR-378a in the aortas of *Klotho* mutant homozygotes (Fig. 6A, (Lovren *et al.*, 2012)). To evaluate the efficacies and persistence of lentiviral transduction, RT-PCR was used to test the aortic levels of miR-145 and miR-378a in mice injected with viruses bearing these miRNAs relative to empty virus vectors. The miR-145 virus raised miR-145a-5p and miR-145a-3p abundances by 1.4±0.8 and 2.0±0.01 fold, respectively, relative to empty virus (Fig. 6B, C). Similarly, miR-378a-5p abundance increased by 1.7±0.04 fold (Fig. 6D) and miR-378a-3p abundance increased by 4.0±4.1 fold (Fig. 6E). Thus this delivery dosage and method successfully augmented aortic miR-145 and miR-378a levels in *Klotho* mutant mice.

### *Increased expression of miR-145 and miR-378a reduced BMP signaling and aortic calcification*

Four different proteins involved in BMP signaling: *Bmp2, Smad1, 5 and 9* are predicted to be targeted by miR-145 (Table 5, Table S3). Therefore, we hypothesized that increased miR-145 levels would repress the synthesis of these pro-osteogenesis factors and ameliorate pathological calcification. Having successfully augmented the level of miR-145 with lentivirus delivery, we evaluated the impact of this treatment on *Bmp2* and *Smad1, 5* and *9* RNA levels with RT-PCR. The *Bmp2* and *Smad5* RNA levels in aortas from mice injected with miR-145-bearing virus fell to 48±0.03% and 65±0.006% ($p=0.002$ and 0.048) that of control aortas from mice injected with empty virus (Fig. 7A, C). The miR-145 virus did not significantly change the abundances of the *Smad1* (Fig. 7B) and *Smad9* (Fig. 7D).

To test if miR-145 overexpression inhibited pathological calcification in *Klotho* homozygous mutant mice, we compared the calcium present in the aortas of *Klotho* homozygous mutant mice injected with empty lentivirus vector or with virus bearing miR-145. The *Klotho* homozygous mutant mice injected with the miR-145 virus had one third less aortic calcium that in the empty virus injected mice (67±0.8%, $p =0.02$, Fig. 7E). Thus, forced miR-145 expression limited pathological calcification in *Klotho* aorta.

The down-regulated miR-378a miRNA is predicted to target *Bmp2* and *Smad5*, but not *Smad1* and *9* (Table 5, Table S3). To evaluate the potiential benefit of restoring miR-378a expression in the aorta of *Klotho* mutant mice, a lentivirus bearing miR-378a was injected. This virus reduced the levels of the target gene RNAs *Bmp2* and *Smad5* to 60±0.02% ($p =0.02$) and 64±0.4% ($p =0.04$) respectively of the RNA levels observed in the mice injected with empty virus (Fig. 8A and B). Finally, treatment with the mir-378a-bearing virus reduced aortic calcium levels by a third (63 ±0.6% of empty control, $p=0.02$) relative to levels in mice exposed to the empty virus (Fig. 8C). Thus as observed for miR-145, forced expression of miR-378a significantly ameliorated pathological calcification of the aorta.

## Discussion

bioRxiv preprint doi: https://doi.org/10.1101/736330; this version posted March 13, 2020. The copyright holder for this preprint (which was not certified by peer review) is the author/funder. All rights reserved. No reuse allowed without permission.



We obtained and analyzed miRNA profiles in aortas from control healthy and *Klotho* homozygous mutant mice with renal impairment that causes aortic calcification. Our unbiased KEGG pathway and GO molecular function term analyses of computationally predicted target genes suggest that many regulated miRNAs influence key signaling processes (Fig. S2 - 5). For the purpose of this report, we focused on miRNAs that were differentially regulated in both sexes (Fig. 4). Among this set, enriched pathways included processes closely involved in osteogenic differentiation in bones and in pathological soft tissue calcification such as the BMP/TGF-beta and WNT/beta-catenin pathways. The target profiles are consistent with the prevailing view that cardiovascular calcification proceeds by known osteogenic mechanisms (Bostrom *et al.*, 2011; Garcia de Vinuesa *et al.*, 2016; Leopold, 2012; Towler, 2017).

We recognize that a fraction of the miRNAs whose levels changed to a statistically significant level were regulated similarly in both male and female mice (Fig. 3C). This is partly explained by a limitation of our study whereby fewer female *Klotho* homozygotes were available (Table 1). The abundances of many miRNAs were changed in the same direction in both male and female mice, but the statistical significance of the change failed to reach our cutoff of $p<0.05$ in both sexes. However, the miRNA profiles between males and females also differ qualitatively. For example, the abundances of miR-17-5p, miR-181c-3p, miR-7019-5p, miR-3069-3p, miR-7685-3p and miR-679-5p changed in opposite directions in males and females (Table 4). Interestingly, a class of miRNAs that modulate epithelial mesenchymal transition (miR-205 and the miR-200 family (Samavarchi-Tehrani *et al.*, 2010)) were highly up-regulated exclusively in the aorta of female mice. MiR-205 and five members of the miR-200 family (miR-141, miR-200a, miR-429) were up-regulated by as much as 154-fold in *Klotho* mutant females but were unchanged in males (Table S2). Epithelial mesenchymal transition influences vascular calcification (Bostrom *et al.*, 2016; Sanchez-Duffhues *et al.*, 2019). Both quantitative and qualitative differences in aortic miRNA profiles in each sex may be highly clinically relevant because there are significant disparities in incidence, prognosis, and response to treatments for arterial diseases between men and women (den Ruijter *et al.*, 2015) We are separately investigating the sex-associated differences in the context of a study aimed at clarifying the impact of sex on BMP signaling (Shah & Rogers, 2018).

We selected two miRNAs, miR-145 and miR-378, to test the principle that miRNAs targeting members of the BMP signaling pathway would reduce aortic calcification. We used the *Klotho* hypomorphic model because the swift pace of aortic calcification in the Klotho mutant homozygotes facilitates testing therapeutic approaches to reducing calcification. In contrast, other models are experimentally time-consuming. For example, mice with genetically sensitized hyperlipidemia backgrounds must be fed special diets for months (Miller *et al.*, 2011; Neven & D'Haese, 2011). In *Klotho* mutant mice with hyperphosphatemia, elevated aortic BMP signaling and calcification is observed at 6-7 weeks of age (Fig. 1, (Gomez-Stallons *et al.*, 2016)). In this model, only 10 days of exposure to viruses overexpressing miR-145 and miR-378 limited aortic calcification (Fig. 7, 8). Studies using *Klotho* mice with renal disease also are relevant to human biology, because KLOTHO deficiency is associated with chronic kidney disease that promotes valve and vascular calcification in people (Arking *et al.*, 2005; Arking *et al.*, 2003; Ichikawa *et al.*, 2007; Koh *et al.*, 2001). This work underscores the

bioRxiv preprint doi: https://doi.org/10.1101/736330; this version posted March 13, 2020. The copyright holder for this preprint (which was not certified by peer review) is the author/funder. All rights reserved. No reuse allowed without permission.



great potential for miRNA-based therapies in treating calcification pathologies.

Restoration of aortic miR-145 levels has also been tested in a different model of vascular calcification. Forced expression of miR-145 reduced atherosclerotic plaque size, increased plaque stability, and promoted a contractile cell phenotype in the *ApoE*, high fat diet mouse model of hyperlipidemia (Lovren *et al.*, 2012). Our demonstration of reduced calcification in *Klotho* mutant homozygous mice with forced miR-145 (Fig. 7) indicates that miR-145 also attenuates vascular disease in a model of atherosclerosis caused by hyperphosphatemia. The effectiveness of this microRNA in these highly dissimilar physiological situations suggest that miR-145 directly promotes vascular health and inhibits pathological osteogenesis.

Like miR-145, miR-378a was significantly down-regulated in blood samples from patients with coronary artery disease compared to healthy subjects (Weber *et al.*, 2011). Furthermore, both miRNAs target regions of the BMP2 and other BMP signaling genes that are highly conserved between mice and humans (Table 5, (Hou *et al.*, 2012; Y. J. Yang *et al.*, 2019)). Interestingly, both miRNAs are subject to editing whereby specific adenosines are post-transcriptionally converted to inosine (Shoshan *et al.*, 2015; Zheng *et al.*, 2014). Inosine base pairs cytosine, not thymine. Manual sequence inspection indicates that editing would increase the complementarity of miR-145 and miR-378a for sites within both the mouse and human *BMP2* messages. Although editing may significantly change miRNA/message interactions, current databases and prediction tools do not facilitate global predictions of how edited miRNAs may impact signaling pathways.

In summary, we have provided a database of the miRNAs that are differentially expressed in healthy mouse aorta relative to aorta calcified due to defective mineral metabolism and kidney function. We also demonstrated that forced expression of miR-145 and miR-378 inhibited RNAs encoding BMP signaling proteins and chronic kidney disease-associated aortic calcification. MiRNA-145 and miR-378 are candidates for translational studies investigating therapies to block vascular calcification.

bioRxiv preprint doi: https://doi.org/10.1101/736330; this version posted March 13, 2020. The copyright holder for this preprint (which was not certified by peer review) is the author/funder. All rights reserved. No reuse allowed without permission.



## References

Agarwal, V., Bell, G. W., Nam, J. W., & Bartel, D. P. (2015). Predicting effective microRNA target sites in mammalian mRNAs. *Elife, 4*. doi:10.7554/eLife.05005

Arking, D. E., Atzmon, G., Arking, A., Barzilai, N., & Dietz, H. C. (2005). Association between a functional variant of the KLOTHO gene and high-density lipoprotein cholesterol, blood pressure, stroke, and longevity. *Circ Res, 96*(4), 412-418. doi:10.1161/01.RES.0000157171.04054.30

Arking, D. E., Becker, D. M., Yanek, L. R., Fallin, D., Judge, D. P., Moy, T. F., . . . Dietz, H. C. (2003). KLOTHO allele status and the risk of early-onset occult coronary artery disease. *Am J Hum Genet, 72*(5), 1154-1161. doi:10.1086/375035

Balachandran, K., Sucosky, P., Jo, H., & Yoganathan, A. P. (2010). Elevated cyclic stretch induces aortic valve calcification in a bone morphogenic protein-dependent manner. *Am J Pathol, 177*(1), 49-57. doi:10.2353/ajpath.2010.090631

Benjamin, E. J., Muntner, P., Alonso, A., Bittencourt, M. S., Callaway, C. W., Carson, A. P., . . . Stroke Statistics, S. (2019). Heart Disease and Stroke Statistics-2019 Update: A Report From the American Heart Association. *Circulation, 139*(10), e56-e528. doi:10.1161/CIR.0000000000000659

Betel, D., Wilson, M., Gabow, A., Marks, D. S., & Sander, C. (2008). The microRNA.org resource: targets and expression. *Nucleic Acids Research, 36*, D149-D153. doi:10.1093/nar/gkm995

Bostrom, K., Watson, K. E., Horn, S., Wortham, C., Herman, I. M., & Demer, L. L. (1993). Bone morphogenetic protein expression in human atherosclerotic lesions. *J Clin Invest, 91*(4), 1800-1809. doi:10.1172/JCI116391

Bostrom, K. I., Rajamannan, N. M., & Towler, D. A. (2011). The regulation of valvular and vascular sclerosis by osteogenic morphogens. *Circ Res, 109*(5), 564-577. doi:10.1161/CIRCRESAHA.110.234278

Bostrom, K. I., Yao, J., Guihard, P. J., Blazquez-Medela, A. M., & Yao, Y. (2016). Endothelial-mesenchymal transition in atherosclerotic lesion calcification. *Atherosclerosis, 253*, 124-127. doi:10.1016/j.atherosclerosis.2016.08.046

Cheng, S. L., Shao, J. S., Charlton-Kachigian, N., Loewy, A. P., & Towler, D. A. (2003). MSX2 promotes osteogenesis and suppresses adipogenic differentiation of multipotent mesenchymal progenitors. *J Biol Chem, 278*(46), 45969-45977. doi:10.1074/jbc.M306972200

Corbett, A. H. (2018). Post-transcriptional regulation of gene expression and human disease. *Curr Opin Cell Biol, 52*, 96-104. doi:10.1016/j.ceb.2018.02.011

den Ruijter, H. M., Haitjema, S., Asselbergs, F. W., & Pasterkamp, G. (2015). Sex matters to the heart: A special issue dedicated to the impact of sex related differences of cardiovascular diseases. *Atherosclerosis, 241*(1), 205-207. doi:10.1016/j.atherosclerosis.2015.05.003

Derwall, M., Malhotra, R., Lai, C. S., Beppu, Y., Aikawa, E., Seehra, J. S., . . . Yu, P. B. (2012). Inhibition of bone morphogenetic protein signaling reduces vascular calcification and atherosclerosis. *Arterioscler Thromb Vasc Biol, 32*(3), 613-622. doi:10.1161/ATVBAHA.111.242594

Fotinos, A., Fritz, D. T., Lisica, S., Liu, Y., & Rogers, M. B. (2016). Competing Repressive Factors Control Bone Morphogenetic Protein 2 (BMP2) in Mesenchymal Cells. *J Cell Biochem, 117*(2), 439-447. doi:10.1002/jcb.25290

bioRxiv preprint doi: https://doi.org/10.1101/736330; this version posted March 13, 2020. The copyright holder for this preprint (which was not certified by peer review) is the author/funder. All rights reserved. No reuse allowed without permission.



Garcia de Vinuesa, A., Abdelilah-Seyfried, S., Knaus, P., Zwijsen, A., & Bailly, S. (2016). BMP signaling in vascular biology and dysfunction. *Cytokine Growth Factor Rev, 27*, 65-79. doi:10.1016/j.cytogfr.2015.12.005

Gomez-Stallons, M. V., Wirrig-Schwendeman, E. E., Hassel, K. R., Conway, S. J., & Yutzey, K. E. (2016). Bone Morphogenetic Protein Signaling Is Required for Aortic Valve Calcification. *Arterioscler Thromb Vasc Biol, 36*(7), 1398-1405. doi:10.1161/ATVBAHA.116.307526

Guntur, A. R., & Rosen, C. J. (2011). The skeleton: a multi-functional complex organ. New insights into osteoblasts and their role in bone formation: the central role of PI3Kinase. *Journal of Endocrinology, 211*(2), 123-130. doi:Doi 10.1530/Joe-11-0175

Hou, X., Tang, Z., Liu, H., Wang, N., Ju, H., & Li, K. (2012). Discovery of MicroRNAs associated with myogenesis by deep sequencing of serial developmental skeletal muscles in pigs. *PLoS One, 7*(12), e52123. doi:10.1371/journal.pone.0052123

Hu, M. C., Shi, M., Zhang, J., Quinones, H., Griffith, C., Kuro-o, M., & Moe, O. W. (2011). Klotho deficiency causes vascular calcification in chronic kidney disease. *J Am Soc Nephrol, 22*(1), 124-136. doi:10.1681/ASN.2009121311

Ichikawa, S., Imel, E. A., Kreiter, M. L., Yu, X., Mackenzie, D. S., Sorenson, A. H., . . . Econs, M. J. (2007). A homozygous missense mutation in human KLOTHO causes severe tumoral calcinosis. *J Clin Invest, 117*(9), 2684-2691. doi:10.1172/JCI31330

Johnson, J. L. (2019). Elucidating the contributory role of microRNA to cardiovascular diseases (a review). *Vascul Pharmacol, 114*, 31-48. doi:10.1016/j.vph.2018.10.010

Karwowski, W., Naumnik, B., Szczepanski, M., & Mysliwiec, M. (2012). The mechanism of vascular calcification - a systematic review. *Med Sci Monit, 18*(1), RA1-11. Retrieved from https://www.ncbi.nlm.nih.gov/pubmed/22207127

Kay, A. M., Simpson, C. L., & Stewart, J. A., Jr. (2016). The Role of AGE/RAGE Signaling in Diabetes-Mediated Vascular Calcification. *J Diabetes Res, 2016*, 6809703. doi:10.1155/2016/6809703

Koh, N., Fujimori, T., Nishiguchi, S., Tamori, A., Shiomi, S., Nakatani, T., . . . Nabeshima, Y. (2001). Severely reduced production of klotho in human chronic renal failure kidney. *Biochem Biophys Res Commun, 280*(4), 1015-1020. doi:10.1006/bbrc.2000.4226

Kuro-o, M., Matsumura, Y., Aizawa, H., Kawaguchi, H., Suga, T., Utsugi, T., . . . Nabeshima, Y. I. (1997). Mutation of the mouse klotho gene leads to a syndrome resembling ageing. *Nature, 390*(6655), 45-51. doi:10.1038/36285

Leopold, J. A. (2012). Cellular mechanisms of aortic valve calcification. *Circ Cardiovasc Interv, 5*(4), 605-614. doi:10.1161/CIRCINTERVENTIONS.112.971028

Lovren, F., Pan, Y., Quan, A., Singh, K. K., Shukla, P. C., Gupta, N., . . . Verma, S. (2012). MicroRNA-145 targeted therapy reduces atherosclerosis. *Circulation, 126*(11 Suppl 1), S81-90. doi:10.1161/CIRCULATIONAHA.111.084186

Malhotra, R., Burke, M. F., Martyn, T., Shakartzi, H. R., Thayer, T. E., O'Rourke, C., . . . Bloch, D. B. (2015). Inhibition of bone morphogenetic protein signal transduction prevents the medial vascular calcification associated with matrix Gla protein deficiency. *PLoS One, 10*(1), e0117098. doi:10.1371/journal.pone.0117098

bioRxiv preprint doi: https://doi.org/10.1101/736330; this version posted March 13, 2020. The copyright holder for this preprint (which was not certified by peer review) is the author/funder. All rights reserved. No reuse allowed without permission.



Miller, J. D., Weiss, R. M., & Heistad, D. D. (2011). Calcific aortic valve stenosis: methods, models, and mechanisms. *Circ Res, 108*(11), 1392-1412. doi:10.1161/CIRCRESAHA.110.234138

Miller, J. D., Weiss, R. M., Serrano, K. M., Castaneda, L. E., Brooks, R. M., Zimmerman, K., & Heistad, D. D. (2010). Evidence for active regulation of pro-osteogenic signaling in advanced aortic valve disease. *Arterioscler Thromb Vasc Biol, 30*(12), 2482-2486. doi:10.1161/ATVBAHA.110.211029

Mohler, E. R., 3rd, Gannon, F., Reynolds, C., Zimmerman, R., Keane, M. G., & Kaplan, F. S. (2001). Bone formation and inflammation in cardiac valves. *Circulation, 103*(11), 1522-1528. Retrieved from https://www.ncbi.nlm.nih.gov/pubmed/11257079

Nagy, E., Eriksson, P., Yousry, M., Caidahl, K., Ingelsson, E., Hansson, G. K., . . . Back, M. (2013). Valvular osteoclasts in calcification and aortic valve stenosis severity. *Int J Cardiol, 168*(3), 2264-2271. doi:10.1016/j.ijcard.2013.01.207

Nakagawa, Y., Ikeda, K., Akakabe, Y., Koide, M., Uraoka, M., Yutaka, K. T., . . . Matsubara, H. (2010). Paracrine osteogenic signals via bone morphogenetic protein-2 accelerate the atherosclerotic intimal calcification in vivo. *Arterioscler Thromb Vasc Biol, 30*(10), 1908-1915. doi:10.1161/ATVBAHA.110.206185

Neven, E., & D'Haese, P. C. (2011). Vascular calcification in chronic renal failure: what have we learned from animal studies? *Circ Res, 108*(2), 249-264. doi:10.1161/CIRCRESAHA.110.225904

Nigam, V., & Srivastava, D. (2009). Notch1 represses osteogenic pathways in aortic valve cells. *J Mol Cell Cardiol, 47*(6), 828-834. doi:10.1016/j.yjmcc.2009.08.008

Osman, L., Yacoub, M. H., Latif, N., Amrani, M., & Chester, A. H. (2006). Role of human valve interstitial cells in valve calcification and their response to atorvastatin. *Circulation, 114*(1 Suppl), I547-552. doi:10.1161/CIRCULATIONAHA.105.001115

Paraskevopoulou, M. D., Georgakilas, G., Kostoulas, N., Vlachos, I. S., Vergoulis, T., Reczko, M., . . . Hatzigeorgiou, A. G. (2013). DIANA-microT web server v5.0: service integration into miRNA functional analysis workflows. *Nucleic Acids Res, 41*(Web Server issue), W169-173. doi:10.1093/nar/gkt393

Rogers, M. B., Shah, T. A., & Shaikh, N. N. (2015). Turning Bone Morphogenetic Protein 2 (BMP2) on and off in Mesenchymal Cells. *J Cell Biochem, 116*(10), 2127-2138. doi:10.1002/jcb.25164

Samavarchi-Tehrani, P., Golipour, A., David, L., Sung, H. K., Beyer, T. A., Datti, A., . . . Wrana, J. L. (2010). Functional genomics reveals a BMP-driven mesenchymal-to-epithelial transition in the initiation of somatic cell reprogramming. *Cell Stem Cell, 7*(1), 64-77. doi:10.1016/j.stem.2010.04.015

Sanchez-Duffhues, G., Garcia de Vinuesa, A., van de Pol, V., Geerts, M. E., de Vries, M. R., Janson, S. G., . . . Ten Dijke, P. (2019). Inflammation induces endothelial-to-mesenchymal transition and promotes vascular calcification through downregulation of BMPR2. *J Pathol, 247*(3), 333-346. doi:10.1002/path.5193

Shah, T. A., & Rogers, M. B. (2018). Unanswered Questions Regarding Sex and BMP/TGF-beta Signaling. *Journal of Developmental Biology, 6*(2). doi:https://doi.org/10.3390/jdb6020014

bioRxiv preprint doi: https://doi.org/10.1101/736330; this version posted March 13, 2020. The copyright holder for this preprint (which was not certified by peer review) is the author/funder. All rights reserved. No reuse allowed without permission.



Shah, T. A., Zhu, Y., Shaikh, N. N., Harris, M. A., Harris, S. E., & Rogers, M. B. (2017). Characterization of new bone morphogenetic protein (Bmp)-2 regulatory alleles. *Genesis, 55*(7). doi:10.1002/dvg.23035

Shoshan, E., Mobley, A. K., Braeuer, R. R., Kamiya, T., Huang, L., Vasquez, M. E., . . . Bar-Eli, M. (2015). Reduced adenosine-to-inosine miR-455-5p editing promotes melanoma growth and metastasis. *Nat Cell Biol, 17*(3), 311-321. doi:10.1038/ncb3110

Taibi, F., Metzinger-Le Meuth, V., M'Baya-Moutoula, E., Djelouat, M., Louvet, L., Bugnicourt, J. M., . . . Metzinger, L. (2014). Possible involvement of microRNAs in vascular damage in experimental chronic kidney disease. *Biochim Biophys Acta, 1842*(1), 88-98. doi:10.1016/j.bbadis.2013.10.005

Towler, D. A. (2017). Commonalities Between Vasculature and Bone An Osseocentric View of Arteriosclerosis. *Circulation, 135*(4), 320-322. doi:10.1161/Circulationaha.116.022562

Vacante, F., Denby, L., Sluimer, J. C., & Baker, A. H. (2019). The function of miR-143, miR-145 and the MiR-143 host gene in cardiovascular development and disease. *Vascul Pharmacol, 112*, 24-30. doi:10.1016/j.vph.2018.11.006

Weber, M., Baker, M. B., Patel, R. S., Quyyumi, A. A., Bao, G., & Searles, C. D. (2011). MicroRNA Expression Profile in CAD Patients and the Impact of ACEI/ARB. *Cardiol Res Pract, 2011*, 532915. doi:10.4061/2011/532915

Wirrig, E. E., Hinton, R. B., & Yutzey, K. E. (2011). Differential expression of cartilage and bone-related proteins in pediatric and adult diseased aortic valves. *J Mol Cell Cardiol, 50*(3), 561-569. doi:10.1016/j.yjmcc.2010.12.005

Yamada, S., & Giachelli, C. M. (2017). Vascular calcification in CKD-MBD: Roles for phosphate, FGF23, and Klotho. *Bone, 100*, 87-93. doi:10.1016/j.bone.2016.11.012

Yang, X., Meng, X., Su, X., Mauchley, D. C., Ao, L., Cleveland, J. C., Jr., & Fullerton, D. A. (2009). Bone morphogenic protein 2 induces Runx2 and osteopontin expression in human aortic valve interstitial cells: role of Smad1 and extracellular signal-regulated kinase 1/2. *J Thorac Cardiovasc Surg, 138*(4), 1008-1015. doi:10.1016/j.jtcvs.2009.06.024

Yang, Y. J., Luo, S., & Wang, L. S. (2019). Effects of microRNA-378 on epithelial-mesenchymal transition, migration, invasion and prognosis in gastric carcinoma by targeting BMP2. *Eur Rev Med Pharmacol Sci, 23*(12), 5176-5186. doi:10.26355/eurrev_201906_18182

Yu, G., Wang, L. G., Han, Y., & He, Q. Y. (2012). clusterProfiler: an R package for comparing biological themes among gene clusters. *OMICS, 16*(5), 284-287. doi:10.1089/omi.2011.0118

Yu, Z., Seya, K., Daitoku, K., Motomura, S., Fukuda, I., & Furukawa, K. (2011). Tumor necrosis factor-alpha accelerates the calcification of human aortic valve interstitial cells obtained from patients with calcific aortic valve stenosis via the BMP2-Dlx5 pathway. *J Pharmacol Exp Ther, 337*(1), 16-23. doi:10.1124/jpet.110.177915

Yutzey, K. E., Demer, L. L., Body, S. C., Huggins, G. S., Towler, D. A., Giachelli, C. M., . . . Aikawa, E. (2014). Calcific aortic valve disease: a consensus summary from

bioRxiv preprint doi: https://doi.org/10.1101/736330; this version posted March 13, 2020. The copyright holder for this preprint (which was not certified by peer review) is the author/funder. All rights reserved. No reuse allowed without permission.



the Alliance of Investigators on Calcific Aortic Valve Disease. *Arterioscler Thromb Vasc Biol, 34*(11), 2387-2393. doi:10.1161/ATVBAHA.114.302523

Zheng, Y., Li, T., Ren, R., Shi, D., & Wang, S. (2014). Revealing editing and SNPs of microRNAs in colon tissues by analyzing high-throughput sequencing profiles of small RNAs. *BMC Genomics, 15 Suppl 9*, S11. doi:10.1186/1471-2164-15-S9-S11

bioRxiv preprint doi: https://doi.org/10.1101/736330; this version posted March 13, 2020. The copyright holder for this preprint (which was not certified by peer review) is the author/funder. All rights reserved. No reuse allowed without permission.



**Table 1. Number of mice (n) used for the miRNA profiling**

| | **Males** | **Females** |
|---|---|---|
| **Group** | **n** | **n** |
| Control (Wt) | 5 | 4 |
| Control (K+) | 2 | 1 |
| *Klotho* mutant (KK) | 5 | 2 |

bioRxiv preprint doi: https://doi.org/10.1101/736330; this version posted March 13, 2020. The copyright holder for this preprint (which was not certified by peer review) is the author/funder. All rights reserved. No reuse allowed without permission.



**Table 2. Reverse Transcription PCR primer sequences**

| Name | Primer Sequence (5'-3') |
|---|---|
| mmu-miR-145a-3p | F: GCGATTCCTGGAAATACTGTTCTTG |
| mmu-miR-145a-5p | F: GTCCAGTTTTCCCAGGAATCCCT |
| mmu-miR-378a-5p | F: CTCCTGACTCCAGGTCCTGTGT |
| mmu-miR-378a-3p | F: ACTGGACTTGGAGTCAGAAGG |
| Mouse *Bmp2* | F: TAGATCTGTACCGCAGGCA<br>R: GTTCCTCCACGGCTTCTTC |
| Mouse *Smad1* | F: GTGTATGAACTCACCAAAATGTGC<br>R: TAACATCCTGCCGGTGGTATTC |
| Mouse *Smad5* | F: AACTTTCACCATGGCTTCCA<br>R: CCAGAAGCTGAGCAAACTCC |
| Mouse *Smad9* | F: CGATCATTCCATGAAGCTGACAA<br>R: TGGGCAAGCCAAACCGATA |
| Mouse *β-actin* | F: CGCCACCAGTTCGCCATGGA<br>R: TACAGCCCGGGGAGCATCGT |

bioRxiv preprint doi: https://doi.org/10.1101/736330; this version posted March 13, 2020. The copyright holder for this preprint (which was not certified by peer review) is the author/funder. All rights reserved. No reuse allowed without permission.



**Table 3. The number and percentage of miRNAs that differed in control relative to *Klotho* homozygotes (KK), p<0.05**

| | **Male** | **Female** |
|---|---|---|
| **Any significant change** | | |
| Increased in KK | 133 (7.0%) | 100 (5.2%) |
| Reduced in KK | 113 (5.9%) | 58 (3.0%) |
| **1.5-fold difference** | | |
| Increased in KK | 88 (4.6%) | 70 (3.7%) |
| Reduced in KK | 62 (3.2%) | 34 (1.8%) |
| **2-fold difference** | | |
| Increased in KK | 57 (3.0%) | 46 (2.4%) |
| Reduced in KK | 30 (1.6%) | 20 (1.0%) |

bioRxiv preprint doi: https://doi.org/10.1101/736330; this version posted March 13, 2020. The copyright holder for this preprint (which was not certified by peer review) is the author/funder. All rights reserved. No reuse allowed without permission.



**Table 4. Relative abundance of miRNAs that were differentially expressed in both male and female *Klotho* homozygous mutant mice as assessed by microarray comparisons.**

| Name | % control in males (p value) | % control in females (p value) |
|---|---|---|
| miR-16-1-3p | 1,344 (0.0001) | 1,331 (0.04) |
| miR-466f-5p | 489 (0.001) | 540 (0.03) |
| miR-669k-5p | 415 (0.00007) | 331 (0.01) |
| miR-7684-3p | 185 (0.002) | 231 (0.003) |
| miR-744-5p | 171 (0.0001) | 294 (0.00008) |
| miR-1930-3p | 156 (0.01) | 312 (0.005) |
| miR-383-5p | 137 (0.02) | 215 (0.02) |
| miR-6929-3p | 127 (0.01) | 167 (0.02) |
| miR-7080-3p | 114 (0.03) | 145 (0.03) |
| miR-7019-5p | 156 (0.03) | 63 (0.045) |
| miR-3069-3p | 143 (0.02) | 55 (0.04) |
| miR-7685-3p | 121 (0.002) | 85 (0.04) |
| miR-679-5p | 113 (0.007) | 86 (0.046) |
| miR-17-5p | 78 (0.02) | 205 (0.03) |
| miR-181c-3p | 42 (0.02) | 263 (0.02) |
| miR-187-5p | 84 (0.01) | 55 (0.02) |
| miR-330-3p | 67 (0.01) | 41 (0.02) |
| miR-187-3p | 65 (0.009) | 29 (0.009) |
| miR-378c | 63 (0.03) | 47 (0.002) |
| miR-193a-3p | 55 (0.0003) | 34 (0.0004) |
| miR-378a-5p | 53 (0.00009) | 38 (0.0004) |
| miR-365-1-5p | 51 (0.04) | 41 (0.02) |
| miR-193b-5p | 46 (0.02) | 15 (0.0003) |
| miR-193b-3p | 45 (0.00003) | 30 (0.00003) |

bioRxiv preprint doi: https://doi.org/10.1101/736330; this version posted March 13, 2020. The copyright holder for this preprint (which was not certified by peer review) is the author/funder. All rights reserved. No reuse allowed without permission.



**Table 5. Sequence alignments between miR-145a-5p, miR-145a-3p, miR-378a-5p and miR-378a-3p and mRNAs encoding BMP signaling proteins**

| Predicted mmu-miR-145a target sites | | Tools | Conservation of site |
|---|---|---|---|
| mu***Bmp2*** 3' UTR<br>**miR-145a-5p** | 737<br>5′...GGGAAUAAUUAGGAAAACUGUGAC...<br>3′ UCCCUAAGGACCCUUUUGAC-CUG | Miranda | Within rodents |
| mu***Bmp2*** 3' UTR<br>**miR-145a-3p** | 580<br>5'...AUAUUCUUCAAUUCUCAGGAAU...<br>3′ GUUCUUGUCAUAAAGGUCCUUA | Miranda | Between rodents, humans, and chicken |
| mu***Bmp2*** 3' UTR<br>**miR-145a-3p** | 748<br>5′...GGAAAACUGUGACUAUGUCAGGAAG...<br>3′ GUUCUUGUCAUAAAGGUCCUUA | Miranda | Within rodents |
| mu***Smad1*** 3' UTR<br>**miR-145a-5p** | 1187<br>5′...GCAGGGUUUUUCUCUACUGGAAA...<br>3′ UCCCUAAGGACCCUUUUGACCUG | Targetscan | Between rodents, mammals, and birds |
| mu***Smad5*** 3' UTR<br>**miR-145a-5p** | 234<br>5'...UUAGCAUUGAUCUUAAACUGGAA...<br>3' UCCCUAAGGACCCUUUUGACCUG | Targetscan | Between mammals |
| mu***Smad9*** 3' UTR<br>**miR-145a-5p** | 754<br>5'...GAGAUGAAGCUGUAG-ACUGGAAG...<br>3' UCCCUAAGGACCCUUUUGACCUG | Targetscan | Within rodents |
| **Predicted mmu-miR-378 target sites** | | | |
| mu***Bmp2*** 3' UTR<br>**miR-378a-5p** | 579<br>5'...UAUAUUCUUCAAUUCUCAGGAAU...<br>3' UGUGUCCUGGACCUCAGUCCUC | Miranda<br>Targetscan | Between rodents, mammals, and birds |
| mu***Bmp2*** 3' UTR<br>**miR-378a-5p** | 751<br>5'...AAACUGUGACUAUGUCAGGAA...<br>3' UGUGUCCUGGACCUCAGUCCUC | Miranda<br>Targetscan | Within rodents |
| mu***Bmp2*** 3' UTR<br>**miR-378a-3p** | 508<br>5'...GUUCACAAGUUCAAGUCCAAA...<br>3' GGAAGACUGAGGUUCAGGUCA | Miranda | Between rodents and humans |
| mu***Smad5*** 3' UTR<br>**miR-378a-5p** | 1156<br>5'...UUUACUUGGCAGCCUUCAGGAAC...<br>3' UGUGUCCUGGACCUCAGUCCUC | Targetscan | Within rodents |

bioRxiv preprint doi: https://doi.org/10.1101/736330; this version posted March 13, 2020. The copyright holder for this preprint (which was not certified by peer review) is the author/funder. All rights reserved. No reuse allowed without permission.



**Fig. 1. BMP signaling and calcification levels in aorta from homozygous *Klotho* mutant mice.** Aortas were isolated from control (C) mice with normal kidney function ($Kl^{+/+}$ and $Kl^{kl/+}$) or mice homozygous ($Kl^{kl/kl}$) for the *Klotho* mutation with renal disease (KK). Average parameter values are presented with standard error measurements (SEM). **A.** BMP signaling levels as assessed by phosphorylated SMAD1/5/9 (pSMAD) levels normalized to total SMAD1/5/9 (tSMAD) (males, n = 3 – 6; females, n = 5 – 7). **B.** Representative western blot panels showing pSMAD1/5/9 and total SMAD1/5/9 levels, males (top) and females (bottom). All female samples were loaded on one gel; however, one mis-loaded lane was excised from the image. **C.** Average calcium levels normalized to protein concentration (males, n = 9 – 18; females, n = 6 – 7). All experiments were repeated at least twice with similar results. ** $p < 0.01$, **** $p < 0.001$. **D, E.** Male littermates *w*ere scanned with an Albira PET/CT Imaging System (Carestream, Rochester, NY) set at 45 kV, 400 µA, and <35 µm voxel size. Voxel intensities in the reconstructed images were evaluated and segmented with VivoQuant image analysis software (version 1.23, inviCRO LLC, Boston MA). The dashed white lines mark mineralized areas of the aortic sinus and ascending aorta present in the heart (**Ht**) of the *Klotho* mutant homozygote **(E)**, but not in the heterozygous control $Kl^{kl/+}$ **(D)**. All images are shown at the same scale.

**Fig. 2. *Bmp2* and *Smad1, 5,* and *9* mRNA abundances in aorta from control and homozygous *Klotho* mutant mice.** Aortas were isolated from control mice bearing the wild type (Wt) or heterozygous (+/*Kl*) *Klotho* genotypes, or diseased (KK) homozygous ($Kl^{kl/kl}$) *Klotho* mice between 40 and 50 days of age. *Klotho* mutant homozygous mice had pathologically calcified aorta. *Bmp2* **(A)** and *Smad1* **(B)** RNA levels did not change. *Smad5* **(C)** and *9* **(D)** RNA levels were significantly increased relative to control mice. The bars indicate the mean value +/- SEM. Solid and hollow circles represent individual male and female values, respectively. * = $p < 0.05$, ** = $p < 0.01$.

**Fig. 3. MicroRNA profiles in the aorta from control and *Klotho homozygous (KK)* mutant mice.** RNA was extracted from the aorta of healthy controls ($Kl^{+/+}$ and $Kl^{kl/+}$) or *Klotho* homozygous ($Kl^{kl/kl}$) mice (KK). Samples were assayed using Affymetrix miRNA version 4.0. Data analysis was performed after Robust Multi-Array Average (RMA) normalization with Transcriptome Analysis Console (TAC). **A, B.** Volcano plots illustrate miRNAs whose abundances differed significantly in aorta from diseased mice compared to control mice ($p < 0.05$). The X axis indicates $\log_2$ fold change and the Y axis indicates $-\log_{10}$ p value. Vertical dotted lines indicate 2-fold change. **C.** The Venn diagram shows the number and percentage of miRNAs differentially expressed in male or female mice or in both out of 1908 miRNAs.

**Fig. 4. Gene Ontology (GO) and KEGG (Kyoto Encyclopedia of Genes and Genomes) analyses of miRNAs down-regulated in both sexes of *Klotho* homozygous mutant mice (Table 4).** The genes potentially targeted by down-

bioRxiv preprint doi: https://doi.org/10.1101/736330; this version posted March 13, 2020. The copyright holder for this preprint (which was not certified by peer review) is the author/funder. All rights reserved. No reuse allowed without permission.



regulated miRNAs were predicted by DIANA TOOLS. **A.** Target genes were grouped into gene pathways using the KEGG database. The y-axis represents the name of the KEGG pathway, and the x-axis represents the number of the genes in a certain pathway. **B.** Target genes were grouped into GO molecular function terms using the GO database. The y-axis represents the name of the GO molecular function term, and the x-axis represents the number of genes associated with each GO molecular function term. Low p adjust values are in red and high p adjust values are in blue. GO terms and KEGG pathways that are directly related to the osteogenic differentiation that occurs in vascular calcification are marked with an asterisk (*).

**Fig. 5. MiR-145 and miR-378a abundances are reduced in the aorta of *Klotho* homozygous mutant mice.** Relative miRNA levels in healthy controls ($Kl^{+/+}$ and $Kl^{kl/+}$) or *Klotho* homozygous ($Kl^{kl/kl}$) mice (**KK**) were assessed by RT PCR normalized against the corresponding U6 expression **(A-D)**. The bars represent the mean value +/- SEM and solid and hollow circles represent individual male and female values, respectively. * = $p < 0.05$, ** = $p < 0.01$, *** = $p < 0.005$.

**Fig. 6. Vascular smooth muscle cell (VSMC)-specific lentivirus treatment increases mir-145 and mir-378a abundance in the aorta of *Klotho* mutant mice. A.** Weaned *Klotho* mutant homozygous mice were treated with empty virus or virus bearing miR-145 or miR-378a pre-miRNAs. This lentiviral construct was previously shown to deliver miR-145 specifically to aortic VSMCs (Lovren *et al.*, 2012). The miR-145a-5p **(B)**, miR-145a-3p **(C)** and miR-378a-5p **(D)**, miR-378a-3p **(E)** abundances were evaluated by real-time PCR and normalized against the corresponding U6 abundance. The bars represent the mean value +/- SEM. Solid and hollow circles represent individual male and female values, respectively. ** = $p < 0.01$, **** = $p < 0.001$.

**Fig. 7. Restoring MiR-145 levels reduces the abundance of RNAs encoding BMP signaling factors and aortic calcification.** Increased mir-145 abundance in *Klotho* mutant mice significantly decreased *Bmp2* **(A)** and *Smad5* **(C)** RNA levels and calcium levels **(E)**. *Smad1* **(B)** and *Smad9* **(D)** RNA levels did not change significantly. The bars represent the mean value +/- SEM. Solid and hollow circles represent individual male and female values, respectively. * = $p < 0.05$, ** = $p < 0.01$.

**Fig. 8. Restoring MiR-378a levels reduces the abundance of RNAs encoding BMP signaling factors and aortic calcification.** Increased mir-378a abundance in *Klotho* mutant mice significantly decreased *Bmp2* **(A)**, *Smad5* **(B)** RNA and calcium levels **(C)**. The bars represent the mean value +/- SEM. Solid and hollow circles represent individual male and female values, respectively. * = $p < 0.05$.

certified by peer review) is the author/funder. All rights reserved. No reuse allowed without permission.

Tang *et al.* Fig. 1

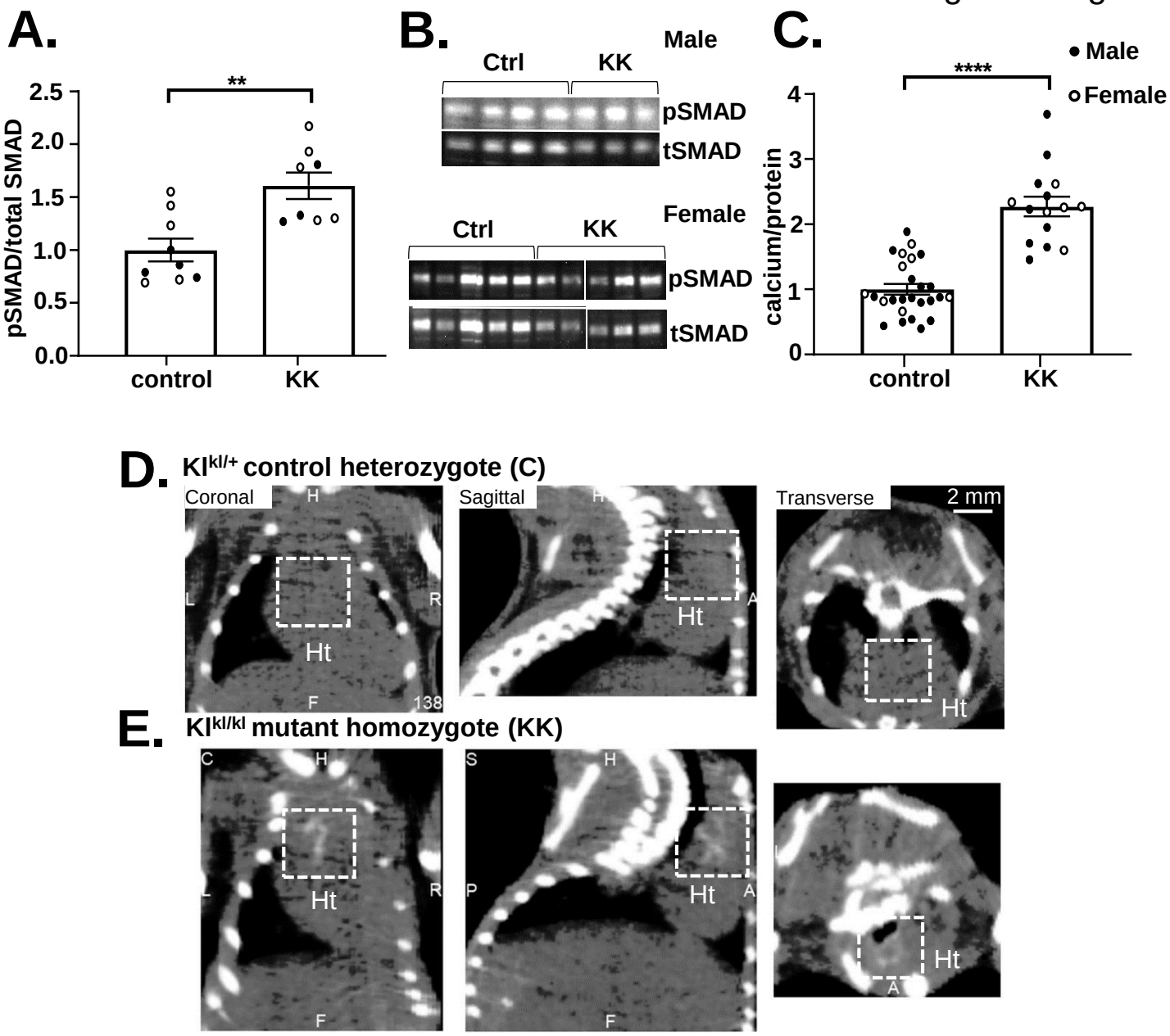

certified by peer review) is the author/funder. All rights reserved. No reuse allowed without permission.

Tang *et al.* Fig. 2

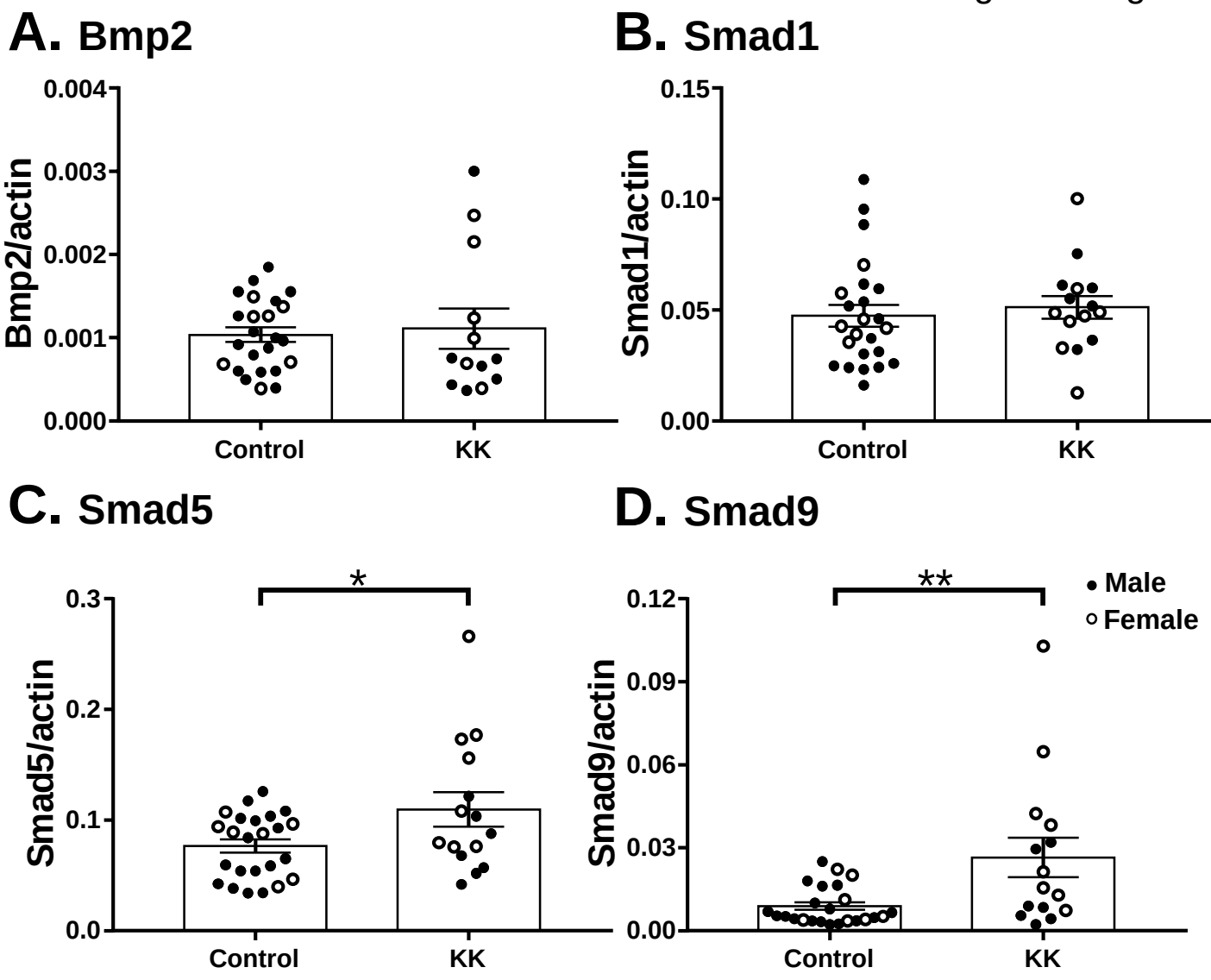

certified by peer review) is the author/funder. All rights reserved. No reuse allowed without permission.



**A.**

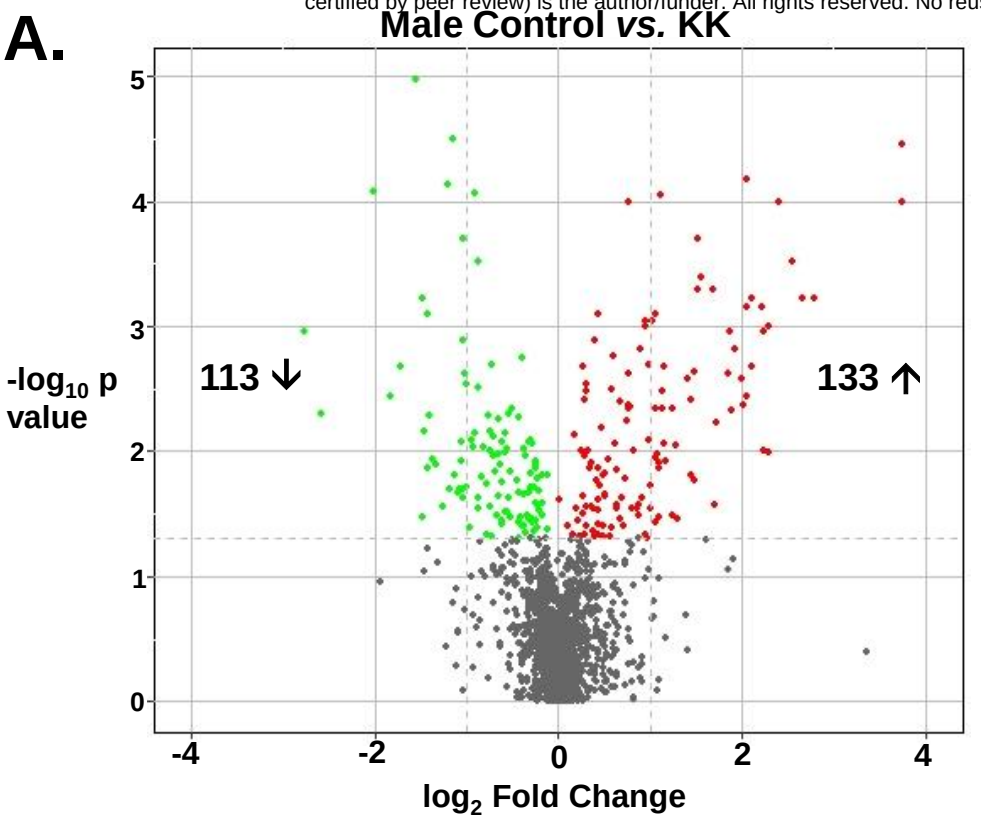


**B.**

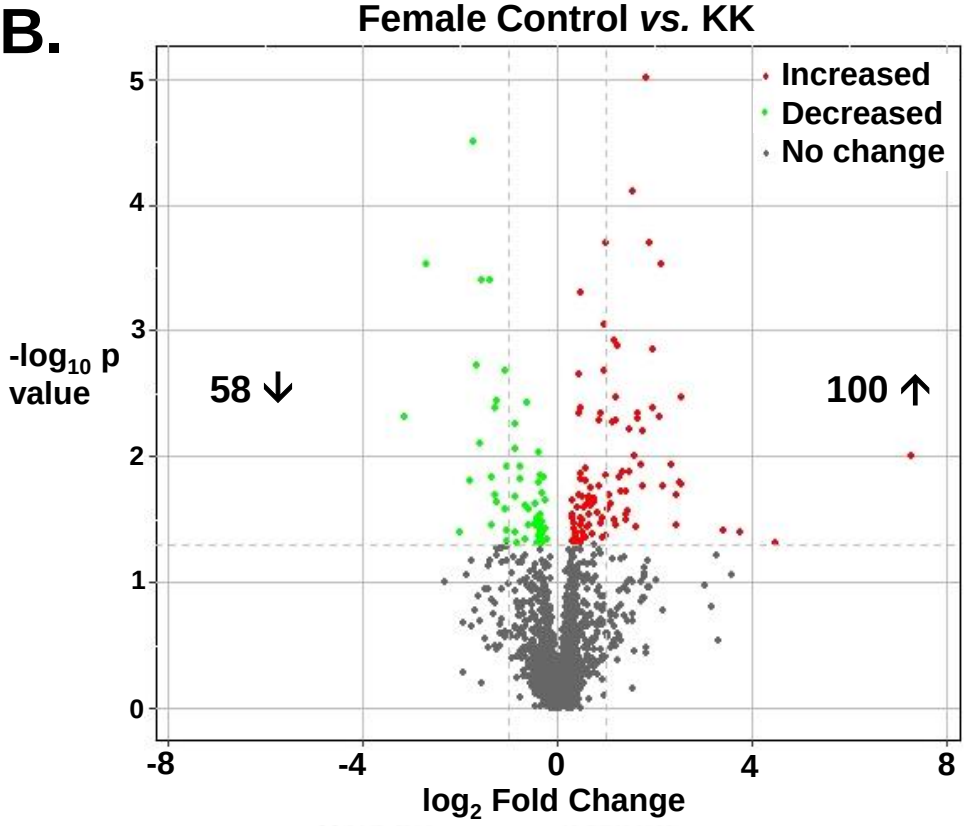


**C**

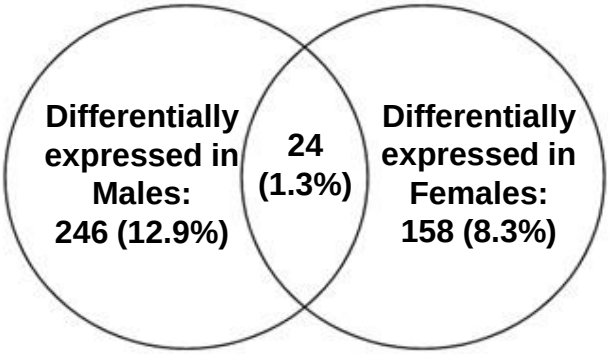

certified by peer review) is the author/funder. All rights reserved. No reuse allowed without permission.

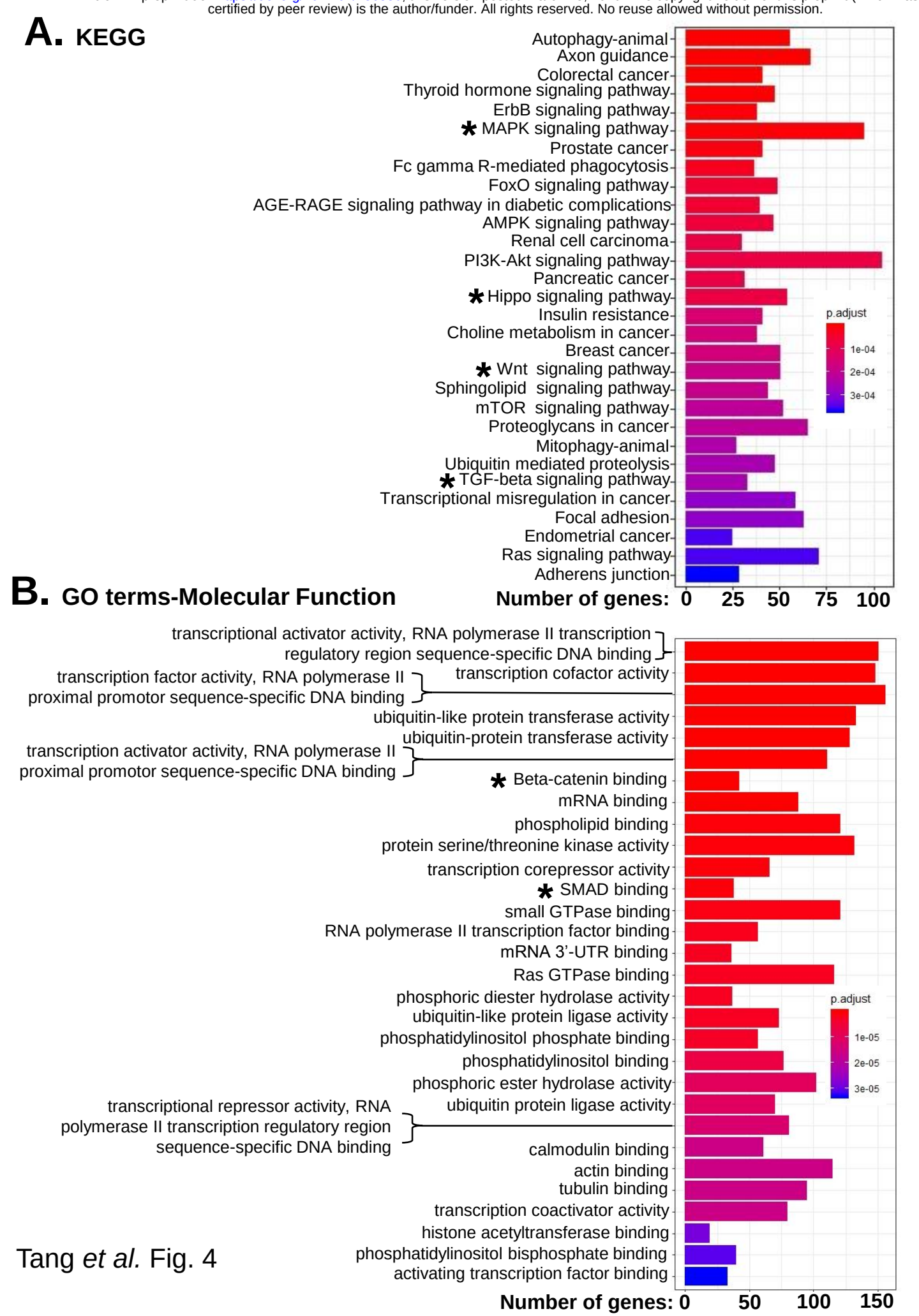


Tang *et al.* Fig. 4

certified by peer review) is the author/funder. All rights reserved. No reuse allowed without permission.



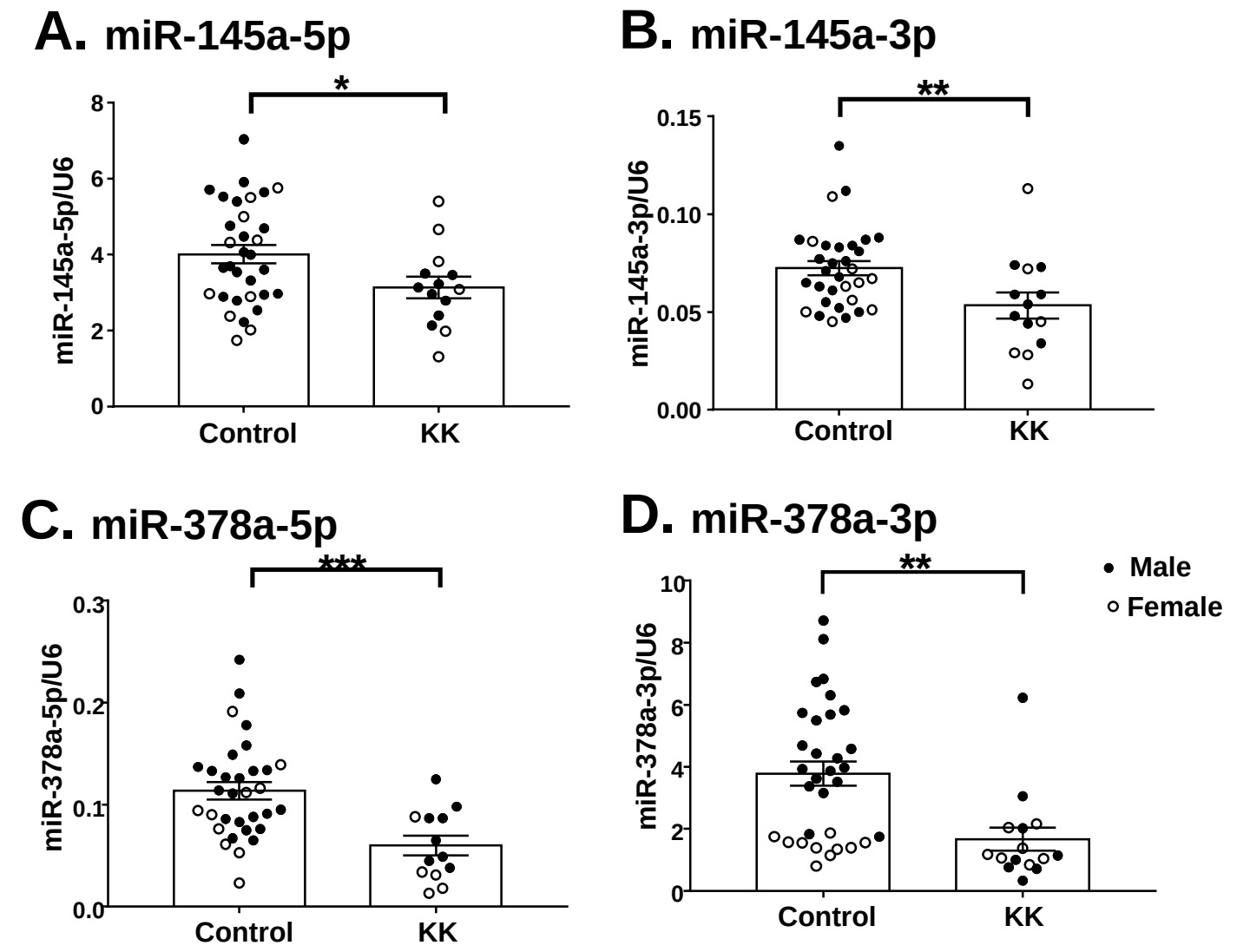

certified by peer review) is the author/funder. All rights reserved. No reuse allowed without permission.



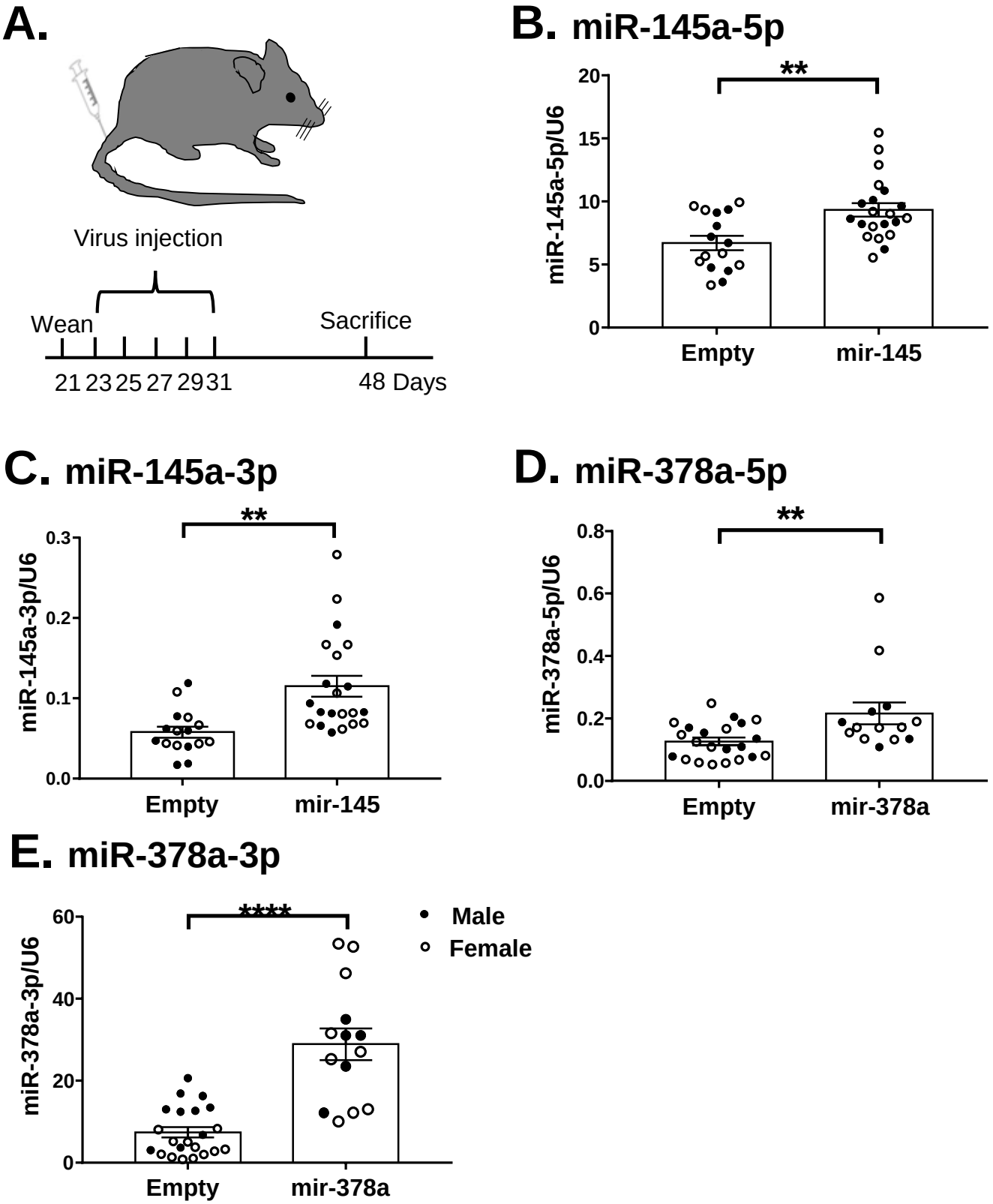

certified by peer review) is the author/funder. All rights reserved. No reuse allowed without permission.

Tang *et al.* Fig. 7

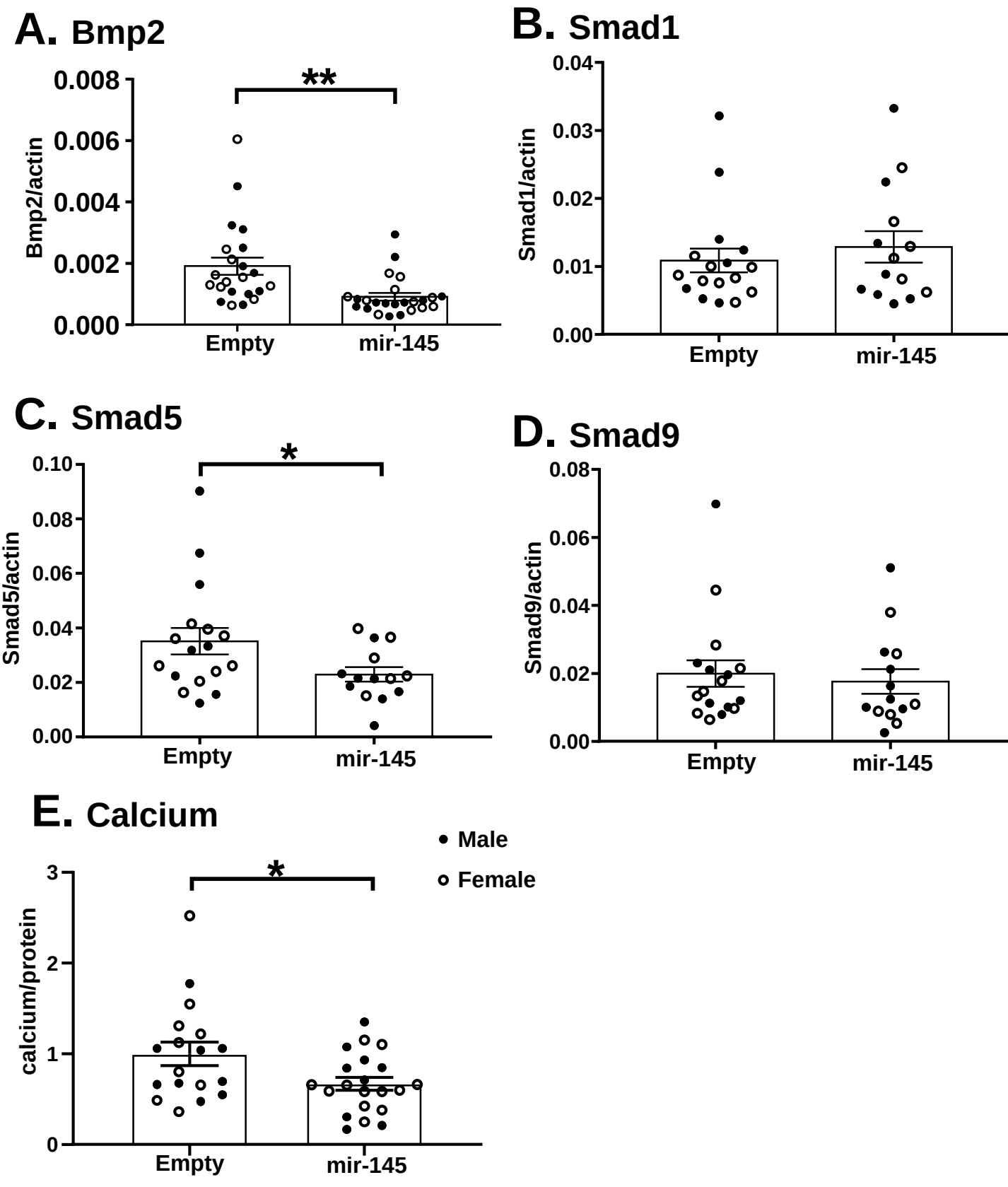

certified by peer review) is the author/funder. All rights reserved. No reuse allowed without permission.



**A. Bmp2**

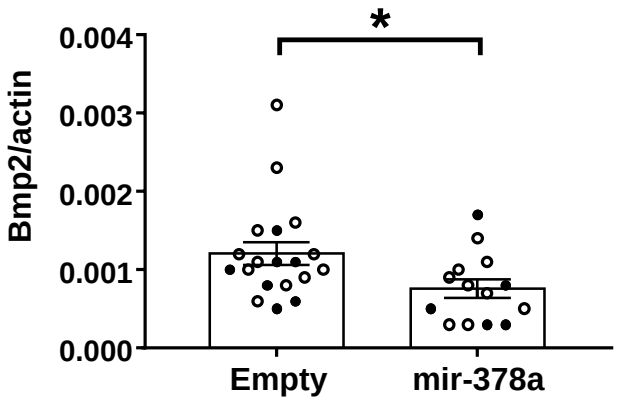


**B. Smad5**

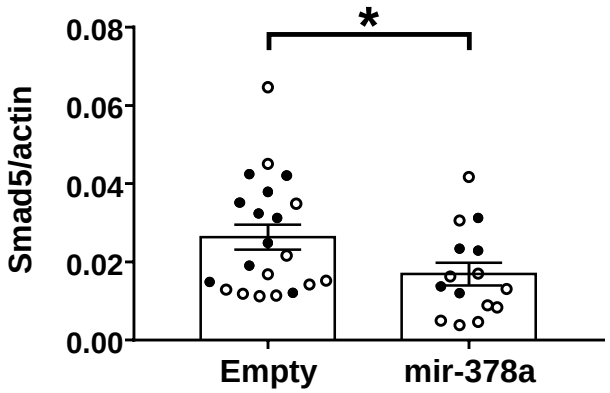


**C. Calcium**